Synchronization of coupled optical microresonators

Jae K. Jang¹, Alexander Klenner¹, Xingchen Ji^{2,3}, Yoshitomo Okawachi¹, Michal Lipson³ and Alexander L. Gaeta¹

The phenomenon of synchronization occurs universally across the natural sciences and provides critical insight into the behaviour of coupled nonlinear dynamical systems. It also offers a powerful approach to robust frequency or temporal locking in diverse applications including communications, superconductors and photonics. Here, we report the experimental synchronization of two coupled soliton mode-locked chip-based frequency combs separated over distances of 20 m. We show that such a system obeys the universal Kuramoto model for synchronization and that the cavity solitons from the microresonators can be coherently combined, which overcomes the fundamental power limit of microresonator-based combs. This study could significantly expand the applications of microresonator combs, and with its capability for massive integration it offers a chip-based photonic platform for exploring complex nonlinear systems.

ynchronization behaviour is ubiquitous in nature¹ and has been studied in a vast variety of systems, such as synchronously flashing fireflies2, pacemaker cells in mammalian hearts3, superconducting Josephson junctions4 and a network of microwave oscillators⁵. Interestingly, the first scientific observation of synchronization dates back to the seventeenth century when Christiaan Huygens discovered that the periods of two pendulum clocks hanging on a common wooden beam tend to lock⁶. He called this observation 'odd sympathy' and suspected that mechanical coupling was responsible for it. Over the course of subsequent studies, it has been confirmed and is now widely accepted that coupling among the constituents of a system plays a key role in their mutual synchronization. This conceptual understanding has been incorporated into several mathematical models¹, most notably the Kuramoto model⁷, with remarkable success and universal applicability. Only in recent years has this concept been extended to optical systems, such as networks of coupled monochromatic lasers, leading to demonstrations of phase-locking8 and coherent beam combining9.

The optical frequency comb represents an electromagnetic excitation composed of a discrete set of equidistant spectral lines, and emerged as an important subfield of optics with numerous applications ranging from spectroscopy to ultrafast optics and metrology¹⁰⁻¹³. Such a source establishes a link between the time-domain description of a uniform pulse train, as might be generated by a mode-locked laser, and the associated 'picket-fence' frequencydomain picture of the laser output spectrum. It is within this context where the possibility of achieving a timing correlation between two mode-locked lasers was initially investigated¹¹. More recently, it has been shown that a microresonator driven by an external single-fre $quency pump field is also capable of generating a frequency comb {}^{14-17}. \\$ The microresonator sustains its comb through nonlinear parametric interactions driven by the external pump and exhibits behaviour that is substantially different to that of mode-locked lasers^{18–24}. Such microresonator-based frequency combs can be mode-locked by the excitation of intracavity dissipative solitary pulses known as temporal cavity solitons (TCSs)25-34 and offer the merits of robustness, compactness and potential for on-chip integration.

Two counter-propagating TCSs can also be excited in a single microresonator, enabling a compact chip-based dual-comb source^{35,36}. As a result of some type of coupling (for example, scattering from the resonator sidewalls), the two solitons have been shown to exhibit a distinct regime in which the repetition rate, and the optical phases, mutually lock. In addition, locking of the comb spacing to an external clocking signal has been reported in a non-soliton parametric comb by means of modulation-induced parametric seeding³⁷, and repetition rate locking of a synchronously pumped Fabry–Pérot microresonator has been demonstrated in which the timing of the circulating TCS locked to that of the pulsed pump³⁸. Despite extensive studies of the dynamics of single microresonators, only recently have there been preliminary theoretical studies exploring evanescently coupled microresonators^{39,40}, which predict frequency-locking between the two generated combs.

Here, we experimentally demonstrate passive synchronization of two microresonator-based optical frequency combs. We generate mode-locked combs in two silicon nitride (Si₃N₄) microresonators on separate chips and synchronize them by coupling a small fraction of one microresonator output to the input of the other microresonator via an optical-fibre link that is 20 m long. In addition, we report on successful coherent combining of the outputs of two synchronized cavity soliton combs, which could have immediate implications in overcoming the power limitation of microresonator comb technology. Using a system of coupled Lugiato–Lefever equations^{41–44}, we find excellent agreement with our experimental results and show that such a system can be reduced to the Kuramoto model. Our demonstration offers the prospect of applications such as the synchronization of multiple-wavelength-division multiplexed sources^{45,46}, synthetic aperture imaging and clock distribution¹³.

Illustration of concept

Our synchronization scheme is illustrated in Fig. 1. For consistency with our experiment, it is assumed that both microresonators are driven by a single pump source. Each microresonator has an integrated microheater, which is electrically tuned to access the modelocked comb state associated with a single TCS³². The heater voltage

ARTICLES NATURE PHOTONICS

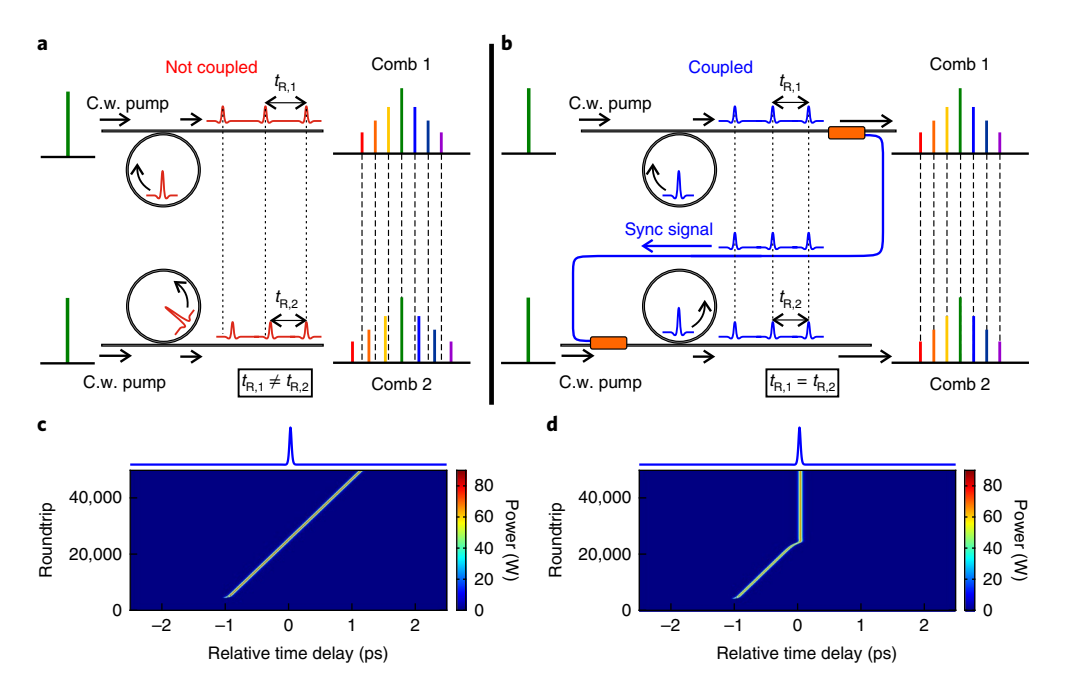


Fig. 1 | **Illustration of the synchronization of microresonator combs. a**, Schematic of the scenario without coupling. The circulating TCS pulses inside the two microresonators have different roundtrip times, $t_{R,1}$ and $t_{R,2}$, which results in the spacings of the two combs being different. **b**, When coupling is established, it is possible to synchronize the pulses and lock the frequencies of the combs such that the comb spacings become identical. **c**, Corresponding numerical simulation showing that the pulse of the slave resonator drifts relative to the reference (master) pulse, shown as a blue curve on top. **d**, Synchronization manifests as stable locking of the relative positions of the TCSs. C.w., continuous-wave.

can also be adjusted after entering the mode-locked state. This thermally shifts resonances⁴⁷ relative to the pump and enables fine tuning of the repetition rate of the circulating TCS or equivalently of the comb spacing (~200 GHz), in each microresonator (see Methods for further information on the experimental set-up). In the absence of physical coupling (Fig. 1a), the microresonators sustain a TCS each, with roundtrip times ($t_{R,1}$ and $t_{R,2}$, which are the reciprocal of the respective repetition rates) that fluctuate relative to each other due to factors such as spatially varying ambient temperature. This mismatch in the roundtrip times is directly correlated to fluctuations in the relative spacing of the associated combs. We establish a coupling link between the microresonators by collecting the output of one microresonator and transmitting a small portion (<1%) of it through an optical-fibre link to the other microresonator (Fig. 1b). The transmitted signal is combined with the pump and the total field drives the second resonator. The first microresonator serves as the reference and constantly transmits a fraction of its output to the other microresonator. Due to this coupling signal, the optical field inside the second microresonator develops localized intensity and phase modulations that enforce synchronization (for a discussion of the physical mechanism see Supplementary Information; Supplementary Figs. 5 and 6). For this reason, we refer to the former and the latter as the master and slave microresonators, respectively, and the coupling signal as the sync signal. We elucidate the dynamics of synchronization in Fig. 1c,d with numerical simulation based on Lugiato-Lefever equations, details of which are described in the Methods and the Supplementary Information. These density plots display the evolutions of the slave TCS without (Fig. 1c) and with (Fig. 1d) coupling with respect to the master TCS (shown as blue curves on top). In both cases, we begin the simulation by seeding the master resonator with an approximate analytic TCS solution^{27,42}. After 5,000 roundtrips, we excite another TCS in the slave resonator. With no coupling, the slave TCS drifts relative to the master TCS at a constant rate numerically chosen to be 0.05 fs per roundtrip, corresponding to a repetition rate mismatch of 2MHz

for a microresonator with 200 GHz free spectral range (FSR). When coupling is introduced, the slave TCS locks its position to that of the master TCS such that their roundtrip times become synchronized. Following the theoretical work of ref. ²⁸ and making appropriate assumptions, we derive (see Supplementary Information) the dynamical equation of the temporal position τ_2 of the enslaved TCS relative to the master TCS, which can be written as

$$\frac{\mathrm{d}\tau_2}{\mathrm{d}t'} = \Delta\tau - k\sin\left(2\pi\frac{\tau_2}{t_{\mathrm{R}~1}}\right) \tag{1}$$

where t' counts the number of roundtrips, $\Delta \tau$ is a relative drift rate per roundtrip in the absence of coupling, k is a coupling constant that depends on the coupling link transmission, and $t_{\rm R,1}$ is the roundtrip time of the master TCS. Equation (1) is mathematically analogous to the Kuramoto model of a system of two oscillators with unidirectional coupling. In this form, equation (1) is also equivalent to Adler's equation, which describes injection locking phenomena Label Predicts that the equilibrium condition (that is, synchronization) can be realized if the coupling strength exceeds the natural drift rate $\Delta \tau$ of the slave TCS.

Results

We experimentally probed the temporal dynamics of synchronization by performing an intensity autocorrelation measurement of the combined comb signals (see Methods and Supplementary Fig. 2). We introduced a translation stage into one of the microresonator outputs to control the relative delay between the two before they combine. We translated the stage over a total range of 1.5 mm, corresponding to one pulse period (~5 ps) of a 200 GHz repetition rate pulse train. Figure 2a shows a series of autocorrelation traces for a range of delays when the two combs are locked via the synchronization process. For each trace, a regular set of primary peaks with a 5 ps period is observed, as expected. What distinguishes these traces

NATURE PHOTONICS ARTICLES

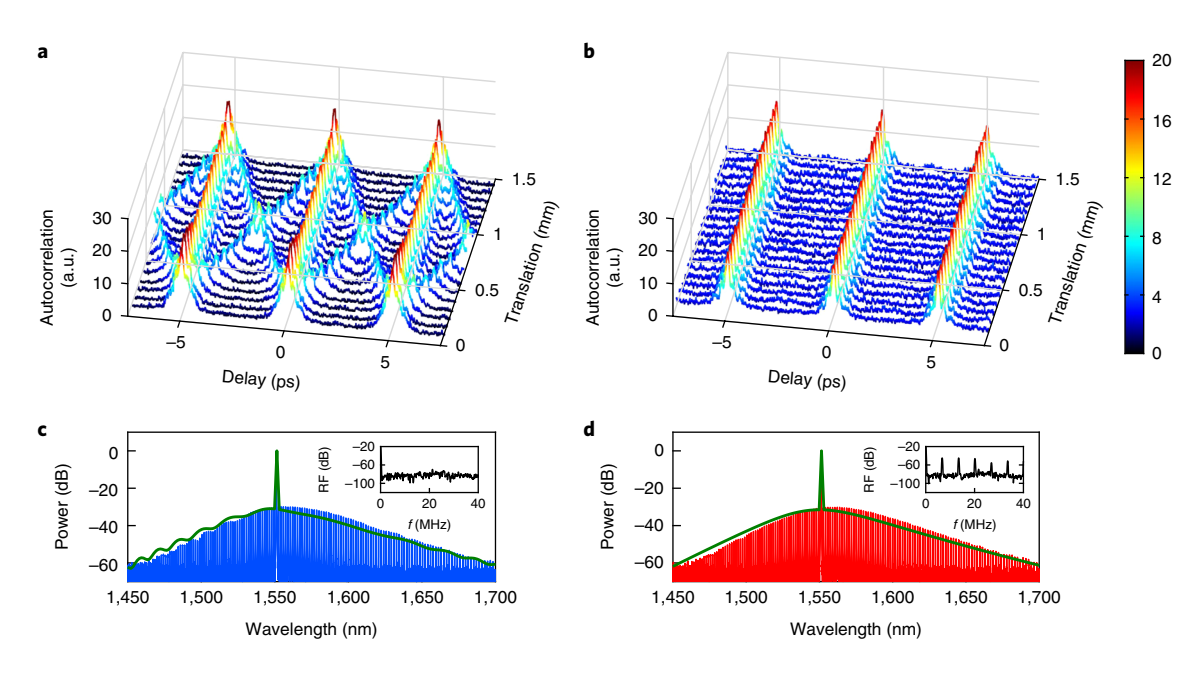


Fig. 2 | Dynamics of synchronization. a,b, Autocorrelation traces of the combined comb signal for synchronized (**a**) and unsynchronized (**b**) cases. When the combs are synchronized, sharp secondary peaks, as well as primary peaks with a 5 ps period, are observed. These secondary peaks can be shifted as the relative delay between the two comb outputs is tuned. **c**, In this case we also observe spectral fringes in the spectrum of the slave comb, and the absence of radiofrequency (RF) beatnotes (inset). When the combs are not synchronized (**b**), no secondary peak is observed and background level is significantly higher. **d**, In this case, the spectral fringes disappear in the optical spectrum and sharp beatnote harmonics appear (inset).

from those of the unsynchronized case in Fig. 2b is the appearance of a symmetric pair of secondary peaks around each primary peak⁵¹. Although each microresonator sustains only one TCS per roundtrip, the combined signal consists of interleaved pulse trains with a relative separation resulting from the output optical path length difference, that is, by how much extra distance the second pulse train must travel compared to the first train before they are combined. The fact that the secondary peaks are well-defined indicates that this relative separation remains stable⁵¹. Varying the delay of one arm enables us to tune the separation. In addition, we present the optical spectrum of the slave comb in Fig. 2c and the complementary frequency downconverted beatnote measurement in the corresponding inset, for the synchronized case. We identify the shallow fringes in the optical spectrum as a signature of synchronization, which we attribute to stable interference between the slave comb and sync signal. Because the fringe spacing is determined by the temporal separation between the comb and the sync signal, such a stationary interference can be observed only if the timing of the circulating TCSs in the two microresonators is synchronized. Note that the fringes are shallow as the optical power of the sync signal is much lower (<1%) than that of the TCS. The absence of beatnotes also implies that the comb lines are spectrally aligned and that the spacings of the combs are identical. The result of numerical simulation, plotted as a green curve in the same panel, is in good agreement with the experiment and confirms the underlying dynamics. In the unsynchronized scenario in Fig. 2b, on the other hand, the secondary peaks disappear, and instead we notice a significant increase in the background level of autocorrelation. Also the fringes of the slave comb disappear, and we simultaneously observe well-defined beatnote harmonics, as displayed in Fig. 2d. The dynamics in this case are analogous to an unstable two-pulse regime with a roundtrip-to-roundtrip fluctuation in the relative positions of the pulses, leading to an increased background level of the autocorrelation traces⁵¹ and to the disappearance of the spectral fringes. The numerical simulation again reveals the underlying dynamics of this scenario.

We present additional experimental evidence of robust comb synchronization in Fig. 3. Here we measure the combined comb spectra with a high-resolution (10 MHz) optical spectrum analyser (Fig. 3a,d). When the combs are synchronized, the spectrum in Fig. 3a exhibits high-contrast modulation and is indistinguishable from the output spectrum of a single microresonator operating in a stable two-pulse regime³². Thus the outputs of the two microresonators are mutually phase-locked and are coherently combined. Moreover, when we zoom in on one of the comb lines corresponding to the 12th line from the pump (enclosed with a dashed box in Fig. 3a), we observe a single comb line as shown in Fig. 3b (blue), which confirms that the spectral lines of the two combs are aligned and that the combs are frequency-locked. This scenario is to be contrasted with the unsynchronized case where no modulation is observed in Fig. 3d, which is a consequence of the drift and fluctuation of the relative intracavity TCS positions. As a result, the roundtrip averaged optical spectrum in Fig. 3d displays no interference pattern. In addition, the expanded plot of the 12th spectral component in Fig. 3b displays two distinct lines (red), as the comb spacings are mismatched. In Fig. 3c, we present the observed variation in the first-harmonic beatnote frequency as the slave resonator is thermally tuned, both in the presence (blue circles) and absence (orange triangles) of coupling (Supplementary Fig. 4). Without coupling, the beatnote frequency decreases smoothly, crosses zero and increases. This trend is contrary to the coupled scenario displaying a total range of 11 mV of heater voltage over which no beatnote is observed (white indicates the synchronized region). Such a frequency-locking regime is analogous to that reported in the context of counter-propagating solitons in a single microresonator^{35,36}. This range of heater voltage corresponds to 400 MHz resonance shift relative to the pump (see Methods for calibration). This result also shows that the allowed comb spacing mismatch between the two combs for this particular coupling strength is ~2.6 MHz or 1.7 MHz, depending on the sign of the mismatch (whether the spacing of the slave comb is larger or smaller than the master resonator). This slight asymmetry arises due to the frequency-dependence of the collection optics and the ARTICLES NATURE PHOTONICS

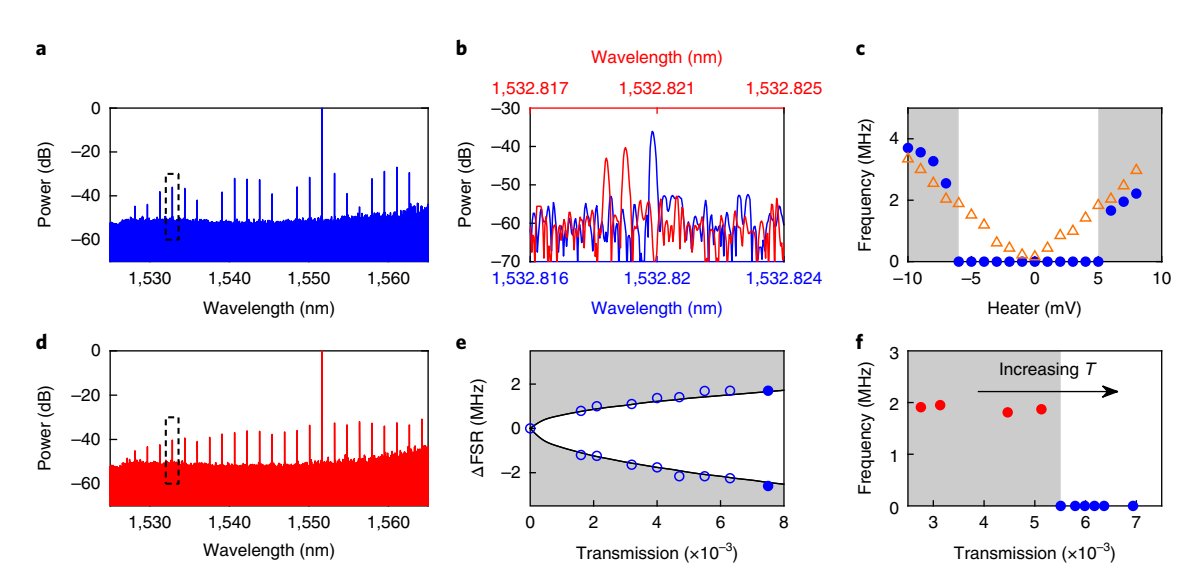


Fig. 3 | Characterization of synchronization behaviour. The results of the synchronized case are plotted in blue and those of the unsynchronized case in red. Grey regions indicate the unsynchronized zones. \mathbf{a} , \mathbf{d} , High-resolution optical spectrum traces of the combined comb for synchronized (\mathbf{a}) and unsynchronized (\mathbf{d}) cases, respectively. \mathbf{b} , Expanded plots of the 12th comb line from the pump, marked by black dashed rectangles in \mathbf{a} and \mathbf{d} . One of the plots has been displaced along the wavelength axis by 0.001 nm for clarity. \mathbf{c} , Fundamental beatnote frequency as the slave resonator is thermally tuned, when the combs are coupled (blue circles) and uncoupled (orange triangles). Orange is used to emphasize that the coupling signal is removed for this measurement. \mathbf{e} , Maximum comb spacing mismatch (ΔFSR) allowed for varying transmission of the sync signal (blue circles) and the corresponding numerical prediction (black curves). Solid circles are derived from \mathbf{c} . \mathbf{f} , Evolution of the beatnote as the coupling strength is varied slowly, showing an abrupt transition to synchronization.

fibre link (Supplementary Fig. 3). These values are in good agreement with the predicted values of 2.5 MHz and 1.5 MHz from our simulations. It has been reported that for a Si₂N₄ microring with 200 GHz FSR, the comb spacing changes with temperature at a rate of -3.57 MHz K⁻¹ (ref. ⁵²), implying that our system can remain synchronized for a temperature difference of >1 K. We show in Fig. 3e that the maximum allowed spacing mismatch depends on the coupling transmission strength, where the simulation (black curves) again correctly predicts the experimental data (blue circles). Finally, we demonstrate the behaviour of the beatnote in Fig. 3f as the coupling transmission is gradually ramped up, while both combs persist. Initially for low coupling strength, the fundamental beatnote is observed at around 2 MHz. It disappears abruptly as coupling is increased, implying the existence of a critical coupling strength for synchronization, as predicted by the Kuramoto model equation (1), and experimentally and numerically in Fig. 3e.

Figure 3a shows that combining two synchronized mode-locked combs can result in stationary interference, which suggests coherent comb combining as a natural application of synchronization. An example of the constructive interference of the individual comb lines, leading to higher comb power, is demonstrated in Fig. 4. We prepared the two individual combs in Fig. 4a,b to have comparable powers before combining them via a beamsplitter. The combined comb spectrum is plotted in blue in Fig. 4c. For comparison, we plot the incoherently combined spectrum in green on the same axis, also recorded after the beamsplitter. For the latter measurement the difference in the repetition rate was thermally set to be 4 MHz, well outside the synchronization range measured in Fig. 3c. Apart from the repetition rate difference, these two measurements were performed under identical conditions. As can be seen, the coherently combined comb has nearly double the power of its incoherent counterpart, and closely matches the expected coherently combined spectral power, theoretically calculated from the spectra in Fig. 4a,b. This demonstration offers a promising approach to boost the overall power of microresonator-based frequency combs. By synchronizing multiple microresonator combs with the technique presented here,

it should be possible to circumvent the output power limitation set by the efficiency of a single microresonator-based comb generator, which has been shown to be of the order of 1% (refs ^{31,33}). As we require less than 1% of the output power of a comb to synchronize it to another, it is possible in principle to boost the power with no significant loss of comb signal.

Conclusion and outlook

We have investigated the synchronization of two microresonatorbased mode-locked frequency combs, and unveiled the underlying dynamics both in the time and frequency domains. This phenomenon can be understood in terms of a coupling-induced interaction between the circulating temporal cavity solitons in the microresonators, leading to their temporal synchronization and, hence, frequency-locking of the associated coherent combs. Based on this new-found knowledge, we have also demonstrated coherent combining of the two mutually synchronized comb. We emphasize that this technique can benefit considerably from the existing technology of photonic integration, which offers superior performance and stability. It should be possible to create a fully integrated on-chip comb generator and combiner, consisting of multiple linked microresonators and interferometers, that would enable power levels far exceeding those typical in single microresonator systems (see Supplementary Information for design details).

Note that, in our experiment, the multiple fibre components add up to 20 m in length to form the coupling link, and there is nothing fundamental about the choice of this length. For the current scheme, we believe that the upper limit of the length is determined by the coherence time $t_{\rm coh}$ of the pump source. For our tunable pump source with a linewidth of ~100 kHz ($t_{\rm coh}$ =10 µs), the synchronization distance is estimated to be ~2 km (of fibre). By using a fixed-frequency pump source with a typical linewidth of less than 1 kHz ($t_{\rm coh}$ > 1 ms), this distance can be increased to 200 km or more. It is only limited by the linewidth of the source laser. As we rely on the thermal tuning of resonances rather than the direct tuning of the laser frequency, the loss of tunability does not pose an issue.

NATURE PHOTONICS ARTICLES

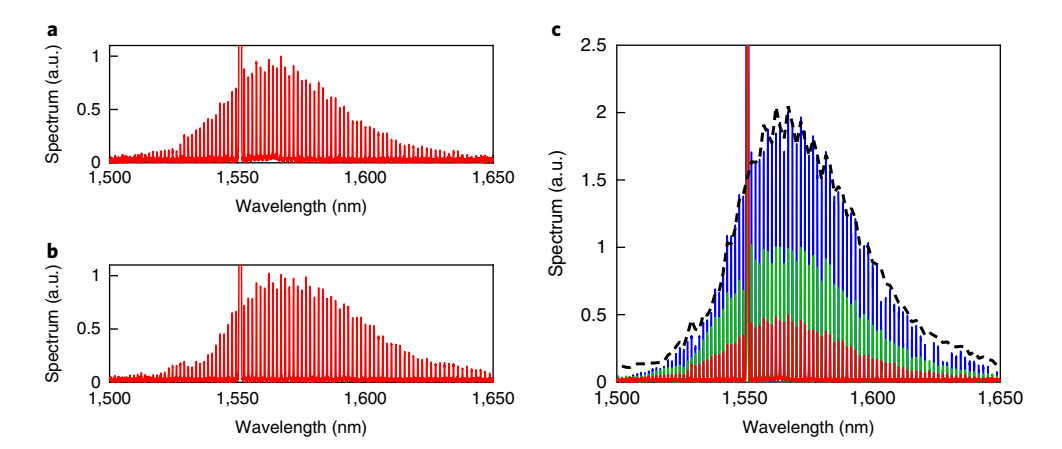


Fig. 4 | Demonstration of coherent comb combining. a,b, Individual comb spectra before they are combined. **c**, Blue curve displays the measured combined spectrum when the combs are synchronized and aligned in time. The black dashed line shows the theoretically anticipated level calculated from the spectra of **a** and **b**. The green curve corresponds to the incoherently combined spectrum. The red curve is identical to the trace in **a**. All comb spectra in **c** are normalized with respect to the incoherently combined spectrum (green).

For synchronization over a large distance, the pump source of the slave resonator can be extracted directly from the coupling signal. As the mode spacing of microresonators is typically of the order of 10–100 GHz, the pump component can be easily isolated from the remaining comb with an optical bandpass filter³⁷, which can be amplified before driving the resonator. In this scenario, the only requirement is that, as discussed above, the distance between the two microresonators be within the coherence length of the source. A potentially interesting aspect for future investigation is to study the interaction of microresonator combs pumped by independent laser sources.

Microresonator combs have sparked interest in data telecommunications^{45,46}, where their functionalities both as wavelengthdivision multiplexing sources on the transmitter end and as local oscillators on the receiver end have been demonstrated⁴⁶. The synchronization technique studied here could further advance such a coherent communication scheme, offering a means of achieving phase coherence between the multi-carrier sources and the local oscillators. Our simulation (Supplementary Figs. 7 and 8) reveals that it is not necessary to use the entire bandwidth of a comb as the sync signal, which implies that the limited bandwidth of an optical amplifier would not be a hindrance to our scheme. In fact, the use of amplifiers can compensate for losses, which could enable applications that require long-distance synchronization, such as aperture imaging and clock distribution¹³. Furthermore, as we have shown, the time-domain dynamics of two coupled microresonators can be reduced to the universal Kuramoto model. Combined with a recent treatment of a single microresonator comb as coupled phase oscillators^{53,54}, this correspondence suggests that microresonator networks can serve as a novel platform for exploring the dynamics of complex systems.

Online content

Any methods, additional references, Nature Research reporting summaries, source data, statements of data availability and associated accession codes are available at https://doi.org/10.1038/s41566-018-0261-x.

Received: 18 April 2018; Accepted: 29 August 2018; Published online: 08 October 2018

References

 Strogatz, S. H. From Kuramoto to Crawford: exploring the onset of synchronization in populations of coupled oscillators. *Physica D* 143, 1–20 (2000).

- Buck, J. Synchronous rhythmic flashing of fireflies. II. Q. Rev. Biol. 63, 265–289 (1988).
- 3. Michaels, D. C., Matyas, E. P. & Jalife, J. Mechanisms of sinoatrial pacemaker synchronization: a new hypothesis. *Circ. Res.* **61**, 704–714 (1987).
- Wiesenfeld, K., Colet, P. & Strogatz, S. H. Synchronization transitions in a disordered Josephson series array. Phys. Rev. Lett. 76, 404–407 (1996).
- York, R. A. & Compton, R. C. Quasi-optical power combining using mutually synchronized oscillator arrays. *IEEE Trans. Microwave Theory Tech.* 39, 1000–1009 (1991).
- Ramirez, J. P., Olvera, L. A., Nijmeijer, H. & Alvarez, J. The sympathy of two pendulum clocks: beyond Huygens observations. Sci. Rep. 6, 23580 (2016).
- Kuramoto, Y. Self-entrainment of a population of coupled non-linear oscillators. In *Proc. Int. Symp. Mathematical Problems in Theoretical Physics* (ed. Araki, H.) 420–422 (Springer, Berlin, 1975).
- Nixon, M. et al. Controlling synchronization in large laser networks. *Phys. Rev. Lett.* 108, 214101 (2012).
- Cheo, P. K., Liu, A. & King, G. G. A high-brightness laser beam from a phase-locked multicore Yb-doped fiber laser array. *IEEE Photon. Technol. Lett.* 13, 439–441 (2001).
- Udem, T., Holzwarth, R. & Hänsch, T. W. Optical frequency metrology. Nature 416, 233–237 (2002).
- Cundiff, S. T. & Ye, J. Colloquium: femtosecond optical frequency combs. Rev. Mod. Phys. 75, 325–342 (2003).
- Dudley, J. M., Genty, G. & Coen, S. Supercontinuum generation in photonic crystal fiber. Rev. Mod. Phys. 78, 1135 (2006).
- Newbury, N. R. Searching for applications with a fine-tooth comb. Nat. Photon. 5, 186–188 (2011).
- Del'Haye, P. et al. Optical frequency comb generation from a monolithic microresonator. *Nature* 450, 1214–1217 (2007).
- Savchenkov, A. A. et al. Tunable optical frequency comb with a crystalline whispering gallery mode resonator. *Phys. Rev. Lett.* 101, 093902 (2008).
- Levy, J. S. et al. CMOS-compatible multiple-wavelength oscillator for on-chip optical interconnects. Nat. Photon. 4, 37–40 (2010).
- Razzari, L. et al. CMOS-compatible integrated optical hyper-parametric oscillator. Nat. Photon. 4, 41–45 (2010).
- Herr, T. et al. Universal formation dynamics and noise of Kerr-frequency combs in microresonators. Nat. Photon. 6, 480–487 (2012).
- Leo, F., Gelens, L., Emplit, P., Haelterman, M. & Coen, S. Dynamics of one-dimensional Kerr cavity solitons. Opt. Express 21, 9180–9191 (2013).
- Parra-Rivas, P., Gomila, D., Matías, M. A., Coen, S. & Gelens, L. Dynamics
 of localized and patterned structures in the Lugiato–Lefever equation
 determine the stability and shape of optical frequency combs. *Phys. Rev. A*89, 043813 (2014).
- Anderson, M., Leo, F., Coen, S., Erkintalo, M. & Murdoch, S. G. Observation of spatiotemporal instabilities of temporal cavity solitons. *Optica* 3, 1071–1074 (2016).
- Bao, C. et al. Observation of Fermi-Pasta-Ulam recurrence induced by breather solitons in an optical microresonator. *Phys. Rev. Lett.* 117, 163901 (2016).
- Yu, M. et al. Breather soliton dynamics in microresonators. Nat. Commun. 8, 14569 (2017).

ARTICLES NATURE PHOTONICS

- Lucas, E., Karpov, M., Guo, H., Gorodetsky, M. L. & Kippenberg, T. J. Breathing dissipative solitons in optical microresonators. *Nat. Commun.* 8, 736 (2017).
- Leo, F. et al. Temporal cavity solitons in one-dimensional Kerr media as bits in an all-optical buffer. Nat. Photon. 4, 471–476 (2010).
- 26. Saha, K. et al. Modelocking and femtosecond pulse generation in chip-based frequency combs. *Opt. Express* 21, 1335–1343 (2013).
- Herr, T. et al. Temporal solitons in optical microresonators. Nat. Photon. 8, 145–152 (2014).
- Jang, J. K., Erkintalo, M., Coen, S. & Murdoch, S. G. Temporal tweezing of light through the trapping and manipulation of temporal cavity solitons. *Nat. Commun.* 6, 7370 (2015).
- 29. Del'Haye, P. et al. Phase steps and resonator detuning measurements in microresonator frequency combs. *Nat. Commun.* **6**, 5668 (2015).
- Liang, W. et al. High spectral purity Kerr frequency comb radio frequency photonic oscillator. Nat. Commun. 6, 7957 (2015).
- Yi, X., Yang, Q.-F., Yang, K. Y., Suh, M.-G. & Vahala, K. Soliton frequency comb at microwave rates in a high-Q silica microresonator. *Optica* 2, 1078–1085 (2015).
- Joshi, C. et al. Thermally controlled comb generation and soliton modelocking in microresonators. Opt. Lett. 41, 2565–2568 (2016).
- 33. Wang, P.-H. et al. Intracavity characterization of micro-comb generation in the single-soliton regime. *Opt. Express* **24**, 10890–10897 (2016).
- Webb, K. E., Erkintalo, M., Coen, S. & Murdoch, S. G. Experimental observation of coherent cavity soliton frequency combs in silica microspheres. *Opt. Lett.* 41, 4613–4616 (2016).
- Yang, Q.-F., Yi, X., Yang, K. Y. & Vahala, K. Counter-propagating solitons in microresonators. Nat. Photon. 11, 560–564 (2017).
- Joshi, C. et al. Counter-rotating cavity solitons in a silicon nitride microresonator. Opt. Lett. 43, 547–550 (2018).
- Papp, S. B., Del'Haye, P. & Diddams, S. A. Parametric seeding of a microresonator optical frequency comb. Opt. Express 21, 17615–17624 (2013).
- Obrzud, E., Lecomte, S. & Herr, T. Temporal solitons in microresonators driven by optical pulses. *Nat. Photon.* 11, 600–607 (2017).
- Wen, Y. H., Lamont, M. R. E. & Gaeta, A. L. Synchronization of multiple parametric frequency combs. OSA Technical Digest Paper FW1D.4 (2014).
- Munns, J. H. D., Walmsley, I. A. & Wen, Y. H. Novel interactions of dissipative Kerr solitons in nonlinear cavity networks. In *Proc. European Conf. Lasers and Electro-Optics and European Quantum Electronics Conferences* EF_1_1 (OSA, Washington DC, 2017).
- Lugiato, L. A. & Lefever, R. Spatial dissipative structures in passive optical systems. *Phys. Rev. Lett.* 58, 2209 (1987).
- Wabnitz, S. Suppression of interactions in a phase-locked soliton optical memory. Opt. Lett. 18, 601–603 (1993).
- Coen, S., Randle, H. G., Sylvestre, T. & Erkintalo, M. Modeling of octavespanning Kerr frequency combs using a generalized mean-field Lugiato– Lefever model. Opt. Lett. 38, 37–39 (2013).
- Chembo, Y. K. & Menyuk, C. R. Spatiotemporal Lugiato–Lefever formalism for Kerr-comb generation in whispering-gallery-mode resonators. *Phys. Rev.* A 87, 053852 (2013).
- Levy, J. S. et al. High-performance silicon-nitride-based multiple-wavelength source. IEEE Photon. Technol. Lett. 24, 1375–1377 (2012).

- Marin-Palomo, P. et al. Microresonator-based solitons for massively parallel coherent optical communications. *Nature* 546, 274–279 (2017).
- Carmon, T., Yang, L. & Vahala, K. J. Dynamical thermal behavior and thermal self-stability of microcavities. *Opt. Express* 12, 4742–4750 (2004).
- 48. Adler, R. A study of locking phenomena in oscillators. *Proc. IRE* 34, 351–357 (1946).
- Del'Haye, P., Beha, K., Papp, S. B. & Diddams, S. A. Self-injection locking and phase-locked states in microresonators-based optical frequency combs. *Phys. Rev. Lett.* 112, 043905 (2014).
- Taheri, H., Eftekhar, A. A., Wiesenfeld, K. & Adibi, A. Anatomy of phase locking in hyperparametric oscillations based on Kerr nonlinearity. *IEEE Photon. J.* 9, 6100911 (2017).
- Trebino, R. Frequency-Resolved Optical Gating: The Measurement of Ultrashort Laser Pulses (Springer, New York, 2000)..
- Xue, X. et al. Thermal tuning of Kerr frequency combs in silicon nitride microring resonators. Opt. Express 24, 687–698 (2016).
- Wen, Y. H., Lamont, M. R. E., Strogatz, S. H. & Gaeta, A. L. Self-organization in Kerr-cavity-soliton formation in parametric frequency combs. *Phys. Rev. A* 94, 063843 (2016).
- Taheri, H., Del'Haye, P., Eftekhar, A. A., Wiesenfeld, K. & Adibi, A. Self-synchronization phenomena in the Lugiato–Lefever equation. *Phys. Rev. A* 96, 013828 (2017).

Acknowledgements

This work was supported by the Air Force Office of Scientific Research (AFOSR) (grant no. FA9550-15-1-0303), the National Science Foundation (NSF) (grant no. CCF-1640108) and the Semiconductor Research Corporation (SRC) (grant no. SRS 2016-EP-2693-A). The authors also thank K. Bergman and R. Polster for lending the high-resolution optical spectrum analyser and autocorrelator.

Author contributions

J.K.J. and A.K. performed experiment. J.K.J. carried out theoretical analysis and numerical simulation, and wrote the manuscript with inputs from all authors. J.K.J., A.K., Y.O. and A.L.G. contributed to the interpretation of data. X.J. fabricated the devices under the supervision of M.L. A.L.G. supervised the overall project.

Competing interests

The authors declare no competing interests.

Additional information

Supplementary information is available for this paper at https://doi.org/10.1038/s41566-018-0261-x.

Reprints and permissions information is available at www.nature.com/reprints.

Correspondence and requests for materials should be addressed to A.L.G.

Publisher's note: Springer Nature remains neutral with regard to jurisdictional claims in published maps and institutional affiliations.

© The Author(s), under exclusive licence to Springer Nature Limited 2018

NATURE PHOTONICS ARTICLES

Methods

Experimental set-up. A detailed schematic of the experimental set-up is presented in Supplementary Fig. 1. We used two Si₃N₄ microring resonators with a waveguide cross-section of 730 × 1,500 nm², on two independent chips. Both microresonators have an FSR of ~200 GHz with a corresponding resonator length of 830 μm. They were fabricated using techniques similar to those reported in ref. 55. We also fabricated an integrated platinum microheater on top of each ring resonator, which allowed us to electrically tune the resonance frequency detuning relative to the pump frequency⁴⁷, and to access the single cavity soliton-based coherent frequency comb state using an arbitrary waveform generator. The pump sources for both microresonators were derived from a single continuous-wave (c.w.) laser (TOPTICA CTL 1550) whose output at 1,551.4 nm was amplified with an erbiumdoped fibre amplifier and was split into two light fields of equal intensity with a 50/50 fused fibre coupler. Each field was coupled to the integrated bus waveguide of a microresonator via a lensed fibre. The output of each microresonator was collected into an optical fibre with a microscope objective and a fibre collimator package. It was split with a 90/10 fibre coupler, where the lower intensity beam was used to monitor the optical spectrum with an optical spectrum analyser (OSA). The remaining beam was spectrally decomposed into its pump and comb components using a fibre dense wavelength-division-multiplexer (DWDM) with ~50 GHz passband centred at 1,551.72 nm. The pump component enabled us to monitor the relative transmission of the microresonator on an oscilloscope, while the comb component was used for a variety of measurements, such as beatnote measurement with an electronic spectrum analyser. In addition, polarization beamsplitters were inserted in the free-space output paths of the resonators, where small fractions (~1%) of light are reflected. We coherently combined the reflected beams with a non-polarizing beamsplitter and detected the combined beam with a 10 MHz resolution OSA (Aragon Photonics BOSA 400).

The comb component of one microresonator was further split into two beams with a 50/50 coupler. One of the split beams, which consisted of a fraction of the collected comb signal, was transmitted through a fibre link before it was combined with the second c.w. pump beam through a DWDM and drove the other microresonator. We installed a polarization controller in the fibre link to ensure that the polarization state of the transmitted comb signal was collinear with that of the second pump. As the fibre link consisted of many fibre components whose combined length was about 15.5 m of standard telecom single-mode fibre (SMF) with an anomalous group-velocity dispersion (GVD) of $\beta_{2.\rm SMF} = -21.4\,\rm ps^2\,km^{-1}$ at 1,551.4 nm, we added 6.8 m of dispersion compensating fibre (DCF; Vascade S1000) with a manufacturer-specified normal GVD coefficient of $\beta_{2.\rm DCF} = 48\,\rm ps^2\,km^{-1}$ for GVD compensation. The total fibre link was 22.3 m in length.

We stabilized the optical path length of the fibre link by detecting the time-dependent interference pattern between the residual pump component of the sync signal and the second c.w. pump. This signal was detected with a photodiode and was split into two signals. One was monitored on the oscilloscope while the other was sent to a commercial proportional-integral controller (New Focus LB1005) to generate an error signal, defined as the difference between the detected signal and the internal reference level. The controller actuated on a fibre stretcher in the link according to the error signal and stabilized the interference signal.

The set-up for autocorrelation measurement is summarized with a simple schematic in Supplementary Fig. 2. It only shows a portion of the set-up that is relevant to autocorrelation measurement, and the rest is identical to the schematic of Supplementary Fig. 1. We added a polarization controller to each input arm of the 50/50 coupler, which allowed independent control over the individual polarization states of the two comb outputs. A fibre-coupled variable delay line was added to one arm to control the relative temporal delay between the two combs. The comb signals were then combined and amplified with an ultrashort optical

pulse amplifier to an average power of about 30 mW. A length of DCF was added after the amplifier to compensate for the GVD of the fibre links. By ensuring that the input arms of the 50/50 coupler were similar in length, we were able to compensate for the GVD of both arms with a single length of DCF. Each trace of Fig. 2a,b in the main text corresponds to a fixed delay between the two arms. The delay is varied in steps of 0.075 mm over a total range of 1.5 mm, covering one pulse period (5 ps) of a 200 GHz pulse train.

Beatnote measurement and synchronization range. After accessing the single cavity soliton regime, the waveform generator supplied a constant d.c. offset to the microheaters to sustain the state. Tuning this offset voltage alters the resonance frequency detuning from the pump^{32,47}, and hence the characteristics of the circulating cavity solitons²⁵. This was the basis of the measurements in Fig. 3c,e. For Fig. 3c, we systematically tuned the heater voltage of the slave microresonator in steps of 1 mV, and for each voltage, acquired the beatnote trace. The master microresonator was left unaltered. The fundamental beatnote was extracted from each trace. For Fig. 3e, this procedure was repeated multiple times for a range of different transmission coefficients of the coupling fibre link. The coupling transmission was varied by inserting different absorptive filters. Additionally, we inserted a 99/1 coupler in the fibre link where the 1% tap allowed us to track the coupling strength without introducing much loss. For each transmission value, we extracted the frequency of the first beatnote detected on either side of the synchronization range. For more details, see Supplementary Fig. 4.

For Fig. 3f, we replaced the absorptive filters with a combination of a half-waveplate and an in-line polarizer, which enabled continuous variation of the transmission. We first set the heater voltage of the slave microresonator such that the fundamental beatnote was observed at $\sim 2\,\mathrm{MHz}$. The beatnotes were detected as we manually rotated the half-waveplate.

Calibration of microheater voltage. To measure the calibration factor between the heater voltage and the corresponding thermal shift of the resonances, we externally modulated the frequency of the c.w. pump laser with a triangular waveform. The total frequency shift in this case was 7.68 GHz. The d.c. heater voltage was adjusted so that the nearest resonance appeared within this range. We measured the resonance shift as the voltage was further varied. From this procedure, we calculated the calibration factor to be 35.6 MHz mV $^{-1}$. Therefore, the synchronization range of 11 mV in Fig. 3c corresponds to an $\sim\!400\,\mathrm{MHz}$ thermal shift of resonance.

Numerical simulation. Our theoretical model is based on a set of Lugiato–Lefever equations $^{41-44}$, which are numerically integrated by employing the split-step Fourier method with a step size corresponding to one roundtrip time of the master resonator. The span of the temporal grid was chosen to be the roundtrip time to satisfy the periodic boundary condition of the resonator. The grid was discretized into n=1,024 points, which is sufficient to describe the full spectral widths of the combs. For more details on the model and parameter values, see Supplementary Information.

Data availability

The data that support the plots within this paper and other findings of this study are available from the corresponding author upon reasonable request.

References

 Ji, X. et al. Ultra-low-loss on-chip resonators with sub-milliwatt parametric oscillation threshold. Optica 4, 619–624 (2017).